AIP | Review of Scientific Instruments

Low temperature and high magnetic field spectroscopic ellipsometry system

Sheng-Kai Su, Liang-Chen Li, Yuen-Wuu Suen, Jau-Yang Wu, Hong-Rong Kuo, Yu-Tai Sung, Chien-Ping Lee, and Oleksandr Voskoboynikov

Citation: Review of Scientific Instruments **85**, 055101 (2014); doi: 10.1063/1.4872355
View online: http://dx.doi.org/10.1063/1.4872355
View Table of Contents: http://scitation.aip.org/content/aip/journal/rsi/85/5?ver=pdfcov
Published by the AIP Publishing

Low temperature and high magnetic field spectroscopic ellipsometry system

Sheng-Kai Su,[1,a)] Liang-Chen Li,[2] Yuen-Wuu Suen,[3,4,b)] Jau-Yang Wu,[1] Hong-Rong Kuo,[3] Yu-Tai Sung,[5] Chien-Ping Lee,[1,2] and Oleksandr Voskoboynikov[1]
[1]*Department of Electronics Engineering and Institute of Electronics, National Chiao Tung University, 1001 University Road, Hsinchu 300, Taiwan*
[2]*Center for Nano Science and Technology, National Chiao Tung University, Hsinchu, Taiwan*
[3]*Department of Physics, National Chung Hsing University, Taichung, Taiwan*
[4]*Institute of Nanoscience, National Chung Hsing University, Taichung, Taiwan*
[5]*National Nano Device Laboratories, Hsinchu, Taiwan*

(Received 14 January 2014; accepted 11 April 2014; published online 1 May 2014)

We report on the design and implementation of a spectral ellipsometer at near-infrared wavelength (700–1000 nm) for samples placed in high magnetic fields (up to 14 T) at low temperatures (∼4.2 K). The main optical components are integrated in a probe, which can be inserted into a conventional long-neck He dewar and has a very long free-space optical path (∼1.8 m×2). A polarizer-sample-(quarter-wave plate)-rotating analyzer configuration was employed. Two dielectric mirrors, one before and one after the sample in the optical path, helped to reflect the light back to the analyzer and a two-axis piezo-driven goniometer under the sample holder was used to control the direction of the reflected light. Functional test results performed on an intrinsic GaAs wafer and analysis on the random error of the system are shown. We obtained both amplitude and phase ellipsometric spectra simultaneously and observed helicity transformation at energies near the GaAs exciton transitions in the phase spectra. Significant shifts of them induced by magnetic fields were observed and fitted with a simple model. This system will allow us to study the collective magneto-optical response of materials and spatial dispersive exciton-polariton related problems in high external magnetic fields at low temperatures. © *2014 AIP Publishing LLC*. [http://dx.doi.org/10.1063/1.4872355]

I. INTRODUCTION

Ellipsometry is considered one of the most sensitive and non-invasive techniques, usually being applied to characterize the optical properties of thin-film materials, such as complex refractive index and thickness.[1–3] The spectroscopic ellipsometry, which measures the optical parameters at different wavelengths, provides additional information on the optical transitions in the material. This is particularly useful for studying semiconductor thin films or nanostructures, where various electronic transitions and excitonic transitions are important. For many of these studies, especially on new phenomena of materials and new structures, it is desirable that these measurements are performed at low temperatures (T) and high magnetic field (B). For example, nonmagnetic semiconductor nano-object based artificial materials have been proposed to exhibit magnetic-material-like collective optical responses which can be revealed by low-T and high-B ellipsometric measurements.[4–8] Another area of interest is the spatial dispersive exciton-polariton related problems,[9–13] for which the obliquely incident geometry of ellipsometry and high-B fields provide extra information of the momentum space parallel to the interfaces and the effect of spin configurations. We believe such a comprehensive study will help to develop the microscopic theory of exciton-polariton behaviors in magnetic fields. Therefore, a versatile but miniature ellipsometer that can be fitted into and operated in a low temperature and high magnetic field environment is of great importance for the studies mentioned above.

A generalized magneto-optical ellipsometry system was proposed by Berger and Pufall[14] to obtain complex refraction index and magneto-optical coupling constant simultaneously. Later, Neuber *et al.*[15] showed a temperature-varying generalized spectral magneto-optical ellipsometer design with a He-flow cryostat and a small electromagnet of a few tens of mT. Schubert *et al.*[16] extended this technique to far-infrared and a higher magnetic field of a few Tesla to characterize the carrier properties of n-GaAs; Hofmann *et al.*[17] further pushed the technique to terahertz frequency range. Mok *et al.*[18] presented a variable-angle vector-magneto-optical generalized ellipsometer with field magnitude up to 400 mT at room temperature. All the previous systems had relatively short optical path designs and were equipped with small coil magnets or split-coil superconducting magnets, which limited the strength of the applied magnetic fields.

In this paper, we report the design and construction of a spectroscopic ellipsometry system that can be inserted into an Oxford long-neck low temperature dewar, which is equipped with a superconducting magnet with field up to 14 T. This ellipsometer employs free space optics to bring the polarized light in and out of the sample stage, which is placed ∼1.6 m deep in the cryostat. Specific mechanical design to control the light beam and stabilize the overall system is presented. We also provide the test data of a semi-insulated GaAs wafer at 4.2 K and show its ellipsometric spectra up to 14 T.

[a)]Electronic mail: shengkai.ee95g@nctu.edu.tw.
[b)]Electronic mail: ysuen@phys.nchu.edu.tw.

II. SYSTEM DESIGN AND OPERATION PRINCIPLE

A. Description of the complete system

To overcome the constraints of the small bore size (50 mm) of the high-field (14 T) superconducting magnet and a long optical path set by the long-neck liquid-Helium dewar with a liquid-nitrogen jacket, we designed a multi-reflection sample stage mounted at the end of an insert. The laser beam is brought in through free-space along the insert. In this way, we are able to maintain a large incident angle and high polarization stability of the laser beam into the sample as required by an ellipsometry system. To make sure the laser beam traveling from the top window of the dewar can go back to the same window after being reflected by the sample at the center of the magnet that is placed near the bottom of the dewar, we use two dielectric mirrors besides the sample under test to form a triple-reflection configuration.

Figure 1 shows the complete schematic diagram of the ellipsometry system. The whole system was constructed as an insert for the low temperature dewar. It consists of a polarization generation part, a polarization detection part, a signal processing part, and a sample stage that holds the sample and the two dielectric mirrors in a low-temperature environment. A Ti-sapphire laser provides the coherent light in the wavelength range of 700 nm–1000 nm and its FWHM linewidth is about 3 Å. The laser beam is first split into two by a beam-sampler. One beam is coupled into a monochromator for wavelength measurement, and the other is coupled into a 10-m long single-mode fiber ended with a collimator. The light out of the collimator passes through a Glan-Laser calcite polarizer with an extinction ratio larger than 10^5 and then becomes a linearly polarized light. One of the laser beams being branched out by the beam-splitter is detected by a silicon photodiode (D1) to monitor the fluctuation of polarization and intensity, while the other beam is guided into the cryogenic dewar through a window at room temperature. The incident beam is reflected by a dielectric mirror before reaching the sample. The outgoing beam is reflected by another dielectric mirror and then goes to the polarization detection part placed outside the dewar. The polarization detection part includes a quarter-wave plate, a rotating analyzer, and another silicon photodiode (D2). The photocurrents from D1 and D2 are measured by lock-in amplifiers and current preamplifiers, respectively, in the signal processing part. All reflections, two from the mirrors and one from the sample, have a 60° incident angle and share the same incident plane, making the incoming beam and outgoing beam parallel to each other. The holder containing the mirrors and sample is attached to a two-axis piezoelectric goniometer which can tune the sample orientation *in situ*.

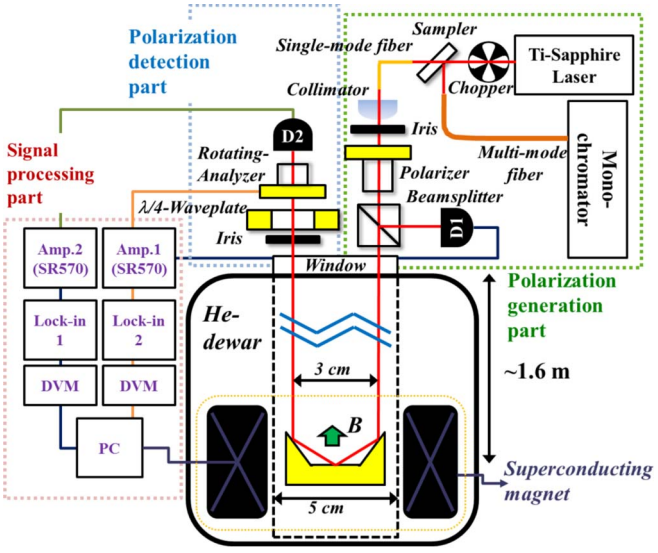

FIG. 1. Schematic diagram of the ellipsometry system, which can be fitted into a long-neck cryogenic dewar with a small-bore high-field superconducting magnet.

B. Operation principle

The polarization state of a light beam can be expressed in the form of Jones vector.[1–3] For a triple-reflection process, the output and input Jones vectors are related by

$$\begin{pmatrix} p_{\text{out}} \\ s_{\text{out}} \end{pmatrix} = \begin{pmatrix} r_{pp}^{\text{C}} & r_{sp}^{\text{C}} \\ r_{ps}^{\text{C}} & r_{ss}^{\text{C}} \end{pmatrix} \begin{pmatrix} r_{pp}^{\text{B}} & r_{sp}^{\text{B}} \\ r_{ps}^{\text{B}} & r_{ss}^{\text{B}} \end{pmatrix} \begin{pmatrix} r_{pp}^{\text{A}} & r_{sp}^{\text{A}} \\ r_{ps}^{\text{A}} & r_{ss}^{\text{A}} \end{pmatrix} \begin{pmatrix} p_{in} \\ s_{in} \end{pmatrix}$$

$$\equiv \begin{pmatrix} r_{pp}^{\text{eff}} & r_{sp}^{\text{eff}} \\ r_{ps}^{\text{eff}} & r_{ss}^{\text{eff}} \end{pmatrix} \begin{pmatrix} p_{in} \\ s_{in} \end{pmatrix} = \mathbf{r}^{\text{eff}} \begin{pmatrix} p_{in} \\ s_{in} \end{pmatrix}, \tag{1}$$

where p and s are the electric field components parallel and perpendicular to the incident plane, and r is the complex reflection coefficient with subscripts and superscripts specifying the polarization states and reflecting materials, respectively. For example, r_{ps}^{B} represents the ratio of the s-component of the light reflected by the sample in the middle and the p-component of the incident light. The effective reflection matrix, $\mathbf{r}^{\text{eff}}$, represents the overall result of all three reflections. The ratio of the output and input ratios of the p- and s- polarization components is defined as[19]

$$\rho = \frac{p_{out}/s_{out}}{p_{in}/s_{in}} = \frac{\left(r_{pp}^{\text{eff}}/r_{ss}^{\text{eff}}\right) + \left(r_{sp}^{\text{eff}}/r_{ss}^{\text{eff}}\right)(p_{in}/s_{in})^{-1}}{1 + \left(r_{pp}^{\text{eff}}/r_{ss}^{\text{eff}}\right)\left(r_{ps}^{\text{eff}}/r_{pp}^{\text{eff}}\right)(p_{in}/s_{in})}$$

$$= \frac{R_{pp}^{\text{eff}} + R_{sp}^{\text{eff}}(p_{in}/s_{in})^{-1}}{1 + R_{pp}^{\text{eff}} R_{ps}^{\text{eff}}(p_{in}/s_{in})}, \tag{2}$$

where[16,19]

$$R_{pp}^{\text{eff}} = \frac{r_{pp}^{\text{eff}}}{r_{ss}^{\text{eff}}} = \tan\Psi_{pp}^{\text{eff}} e^{i\Delta_{pp}^{\text{eff}}}, \tag{3a}$$

$$R_{sp}^{\text{eff}} = \frac{r_{sp}^{\text{eff}}}{r_{ss}^{\text{eff}}} = \tan\Psi_{sp}^{\text{eff}} e^{i\Delta_{sp}^{\text{eff}}}, \tag{3b}$$

$$R_{ps}^{\text{eff}} = \frac{r_{ps}^{\text{eff}}}{r_{pp}^{\text{eff}}} = \tan\Psi_{ps}^{\text{eff}} e^{i\Delta_{ps}^{\text{eff}}}, \tag{3c}$$

$\tan\Psi$ and Δ stand for the amplitude ratio and the phase difference of the reflectivities.

To extract the reflection information from the triple-reflection measurement, we must obtain the effect of the dielectric mirrors first. This can be done through a calibration procedure by using three identical mirrors, i.e., using the same

dielectric mirror (M) to replace the sample. The overall result of the three identical reflections then has the form

$$\begin{pmatrix} \left(r_{pp}^{\mathrm{M}}\right)^3 + 2f_{pp}^{\mathrm{M}} + f_{ss}^{\mathrm{M}} & r_{sp}^{\mathrm{M}} F^{\mathrm{M}} \\ r_{ps}^{\mathrm{M}} F^{\mathrm{M}} & \left(r_{ss}^{\mathrm{M}}\right)^3 + 2f_{ss}^{\mathrm{M}} + f_{pp}^{\mathrm{M}} \end{pmatrix}, \tag{4}$$

where $f_{pp}^{\mathrm{M}} = r_{pp}^{\mathrm{M}} r_{ps}^{\mathrm{M}} r_{sp}^{\mathrm{M}}$, $f_{ss}^{\mathrm{M}} = r_{ss}^{\mathrm{M}} r_{ps}^{\mathrm{M}} r_{sp}^{\mathrm{M}}$, and $F^{\mathrm{M}} = (r_{pp}^{\mathrm{M}})^2 + r_{ps}^{\mathrm{M}} r_{sp}^{\mathrm{M}} + r_{pp}^{\mathrm{M}} r_{ss}^{\mathrm{M}} + (r_{ss}^{\mathrm{M}})^2$. Here we assume the reflection coefficients to be the same due to the same material and identical incident angle. The ellipsometry parameters for each mirror can be obtained with neglecting the product of $r_{ps}^{\mathrm{M}} r_{sp}^{\mathrm{M}}$ terms that are at least three orders smaller than the product of diagonal terms in general:

$$R_{pp}^{\mathrm{M}} = \left(R_{pp}^{\mathrm{cal}}\right)^{1/3}, \tag{5a}$$

$$R_{sp}^{\mathrm{M}} = R_{sp}^{\mathrm{cal}}\left[\left(R_{pp}^{\mathrm{cal}}\right)^2 + R_{pp}^{\mathrm{cal}} + 1\right]^{-1}, \tag{5b}$$

$$R_{ps}^{\mathrm{M}} = R_{ps}^{\mathrm{cal}}\left[\left(R_{pp}^{\mathrm{cal}}\right)^{-2} + \left(R_{pp}^{\mathrm{cal}}\right)^{-1} + 1\right]^{-1}. \tag{5c}$$

The superscript "cal" represents the three identical mirror calibration measurement.

For a measurement where the second mirror is replaced by a sample (σ), the effective reflectivity matrix becomes

$$\begin{pmatrix} \left(r_{pp}^{\mathrm{M}}\right)^2 r_{pp}^{\sigma} & r_{pp}^{\mathrm{M}} r_{ss}^{\mathrm{M}} r_{sp}^{\sigma} + g_{sp} \\ g_{ps} + r_{pp}^{\mathrm{M}} r_{ss}^{\mathrm{M}} r_{ps}^{\sigma} & \left(r_{ss}^{\mathrm{M}}\right)^2 r_{ss}^{\sigma} \end{pmatrix}, \tag{6}$$

where $g_{sp/ps} = r_{sp/ps}^{\mathrm{M}}\,(\mathrm{r}_{ss}^{\mathrm{M}}\,\mathrm{r}_{ss}^{\sigma} + \mathrm{r}_{pp}^{\mathrm{M}}\,\mathrm{r}_{pp}^{\sigma})$. The ellipsometry parameters of the sample (σ) are then obtained by Eq. (3) as

$$R_{pp}^{\sigma} = \frac{R_{pp}^{\mathrm{eff}}}{\left(R_{pp}^{\mathrm{M}}\right)^2}, \tag{7a}$$

$$R_{sp}^{\sigma} = \left[R_{sp}^{\mathrm{eff}} - R_{sp}^{\mathrm{M}}\left(1 + \frac{R_{pp}^{\mathrm{eff}}}{R_{pp}^{\mathrm{M}}}\right)\right]\left(R_{pp}^{\mathrm{M}}\right)^{-1}, \tag{7b}$$

$$R_{ps}^{\sigma} = \left[R_{ps}^{\mathrm{eff}} - R_{ps}^{\mathrm{M}}\left(1 + \frac{R_{pp}^{\mathrm{M}}}{R_{pp}^{\mathrm{eff}}}\right)\right] R_{pp}^{\mathrm{M}}. \tag{7c}$$

The mirror contributions R_{pp}^{M}, R_{sp}^{M}, and R_{ps}^{M} can be deduced from the three-mirror calibration procedure (Eq. (5)).

C. Mechanical design

The main part of the ellipsomety system is designed as a long insert to fit in an Oxford He dewar. Because of the long distance (~1.6 m) between the center of magnetic field and the outlet window and the extreme conditions in the dewar, the mechanical design of the ellipsometer has to be done very carefully to ensure stable operation and ruggedness under harsh conditions. It also needs to be flexible enough to allow fine adjustment of the optical path to make sure that the light beam travels through free space to the sample and back to the polarization detection part accurately. The main mechanical support of the insert is provided by four parallel 6 mm-outside-diameter stainless-steel tubes, which are kept in place and separated by several aluminum spacer plates. In each of the spacer plate, there are two cross-shaped holes to allow the laser beams to go through. Such a frame structure avoids the possibility of bending the insert frame and also suppresses mechanical vibrations.

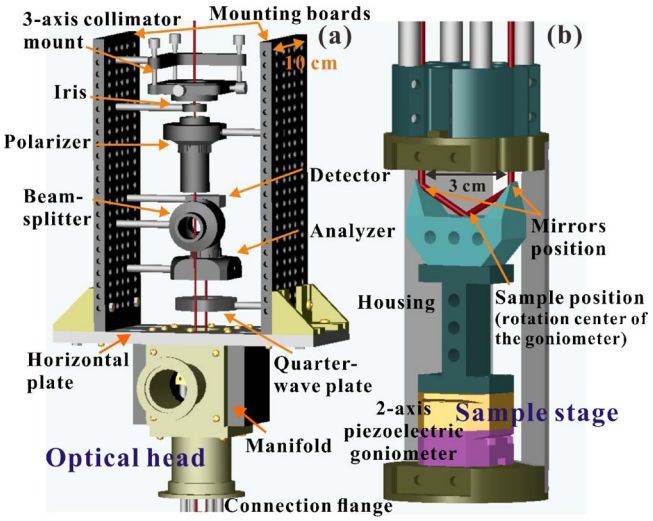

FIG. 2. Design of the ellipsometer insert. (a) The optical head consists of all polarization optical elements in the room temperature environment. (b) The bottom of the insert, positioned in 4.2 K environment, includes a sample stage, a two-axis piezoelectric goniometer, and a protective housing.

The top of the frame structure, as shown in Fig. 2(a), is connected to a manifold that supports the optical head and provides necessary ports for pumping and electrical feedthroughs. The optical head mainly consists of two 25 cm × 10 cm × 1 cm parallel optical breadboards that hold the optical components and detectors.

The bottom of the insert, as shown in Fig. 2(b), includes a sample stage, a two-axis piezoelectric goniometer, and a protective housing, which are all made of titanium. Between components of different materials, beryllium-copper washers are used to reduce the deformation caused by different contractions at low temperatures. To ensure the reflected beam reaching the polarization detection part, the sample stage is mounted on a two-axis piezoelectric goniometer with its rotation center coinciding with the sample position to provide a very precise and instantaneous angle-control without sample displacement.

A thin-wall stainless steel jacket with a 50 mm inner diameter is used to protect the insert and also allows the sliding seal to be used during cooling. The outer jacket must be fit to the insert by carefully tuning the 8 screws in the connection flange on the manifold to avoid any contact between them. Four springs are placed below the horizontal plate of the optical head to counterbalance the weight of the whole insert and also buffer the vibration from the dewar.

D. Data acquisition and reduction

Figure 3 shows the data acquisition procedure. The parameters including the polarizer angle P, the ranges and the steps of the laser wavelength, and the magnetic field are set at the beginning. The superconducting magnet can be switched to the persistent mode to save Helium consumption once

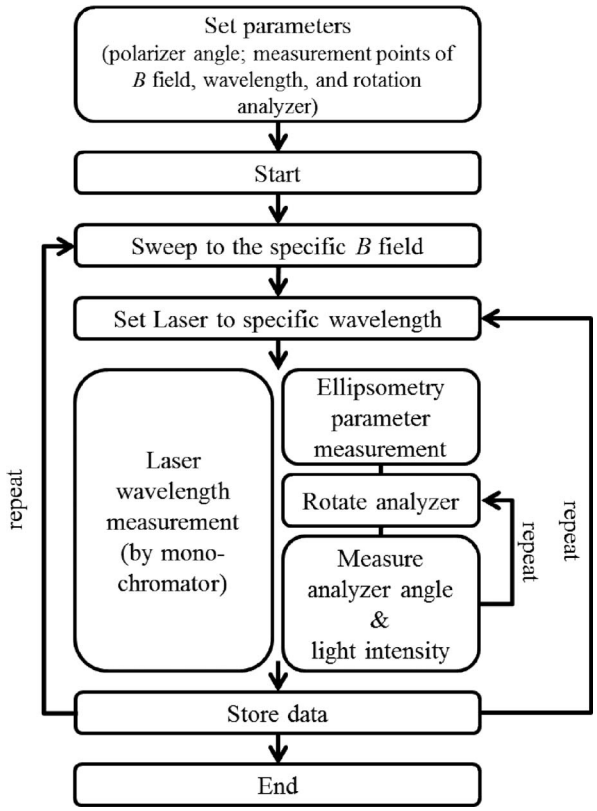

FIG. 3. Flowchart of the data acquisition.

the field strength reaches the setting value. The wavelength of the Ti-sapphire laser is auto-controlled by a step motor and is characterized by a monochromator together with the ellipsometry parameter measurement.

A polarizer-sample-rotating analyzer ellipsometry (RAE) configuration is used to measure the ellipsometry parameters. The measured light intensity can be expressed as[1–3,19]

$$I(P, A) = |E_{in}|^2 |r_{ss}|^2 \cos^2 P |(R_{pp} + R_{sp} \tan P) \cos A + (R_{ps} R_{pp} + \tan P) \sin A|^2, \quad (8)$$

where E_{in} is the complex amplitude of the electric field before the polarizer. A and P are the angles between the incident plane and the analyzer and polarizer transmission axes, respectively. This equation can be further simplified to

$$I(P, A) = I_D[1 + \alpha \cos(2A) + \beta \sin(2A)], \quad (9a)$$

where[19]

$$\alpha = \frac{|R_{pp} + R_{sp} \tan P|^2 - |R_{ps} R_{pp} + \tan P|^2}{|R_{pp} + R_{sp} \tan P|^2 + |R_{ps} R_{pp} + \tan P|^2}, \quad (9b)$$

and

$$\beta = \frac{2Re\{(R_{pp} + R_{sp} \tan P)(R_{sp} R_{pp} + \tan P)\}}{|R_{pp} + R_{sp} \tan P|^2 + |R_{ps} R_{pp} + \tan P|^2}. \quad (9c)$$

The ellipsometry parameters depend only on α and β, and are independent of the average intensity I_D. We can obtain α and β from the Fourier expansion of $I(P, A)$:[20]

$$I_D = \frac{1}{N} \sum_{i=1}^{N} I_i, \quad (10a)$$

$$\alpha = \frac{2}{I_D N} \sum_{i=1}^{N} I_i \cos 2A_i, \quad (10b)$$

$$\beta = \frac{2}{I_D N} \sum_{i=1}^{N} I_i \sin 2A_i, \quad (10c)$$

where I_i is the intensity at A_i, and N is the total number of analyzer angles measured. We can follow the maturely developed method[16,19] by choosing several azimuthal settings P and using Eq. (9) to determine all the ellipsometry parameters R_{pp}, R_{ps}, and R_{sp}.

In some of our studies, the R_{pp} response function near the exciton transition energy at low temperatures and high magnetic fields is important. The contribution from measured R_{ps} and R_{sp} to R_{pp} spectra is small and does not influence the data fitting and interpretation shown in Sec. III. For simplicity and clarity, we will focus on the response of R_{pp} and neglect R_{ps} and R_{sp} in the following data analysis. Equations (9b) and (9c) become the same as in the standard ellipsometry situation.[1–3]

$$\alpha = \frac{\tan^2 \Psi_{pp} - \tan^2 P}{\tan^2 \Psi_{pp} + \tan^2 P}, \quad (11a)$$

and

$$\beta = \frac{2 \tan P \tan \Psi_{pp} \cos \Delta_{pp}}{\tan^2 \Psi_{pp} + \tan^2 P}. \quad (11b)$$

III. MEASUREMENTS AND DISCUSSION

A. Sample preparation and measurement procedure

Since many interesting III-V semiconductor nanostructures are grown on GaAs substrates, we first applied the low temperature and high magnetic field ellipsometry system to characterize the properties of a semi-insulating GaAs (100) substrate (thickness ~330 μm) in the spectral range near its band edge. Two semi-insulating GaP substrates were used as the dielectric mirrors because GaP's bandgap is larger than GaAs's and its refractive index is also reasonably large. In addition, no significant photo- and magneto-optical response is observed for GaP under magnetic fields in the measuring spectral range. The two GaP mirrors and GaAs sample were mounted on the sample stage carefully by grease. To compensate the thickness difference of GaP and GaAs substrates, a glass slide was placed under the GaAs substrate.

The optical alignment procedure was carried out by fine tuning the three-axis collimator mounted on the top of the optical head for the input light beam and the two-axis piezoelectric goniometer at the bottom of the sample stage (see Fig. 2) for the reflected light beam. After the alignment procedure, the probe was carefully sealed by an outer jacket with an O-ring and bolts, and the whole insert was pumped down to ~5 $\times 10^{-5}$ mbar. Before the probe being inserted into the dewar, ~25 mbar Helium gas was introduced into the insert for heat exchange. In the cooling procedure, the insert was lowered down into the low temperature dewar slowly via a sliding seal and the goniometer was simultaneously adjusted to ensure the reflected light traveling back to the photodiode (D2).

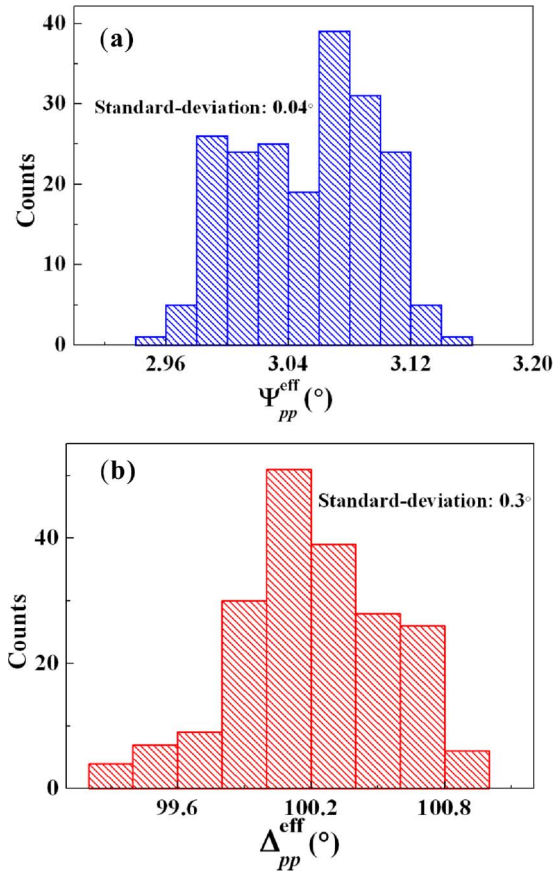

FIG. 4. Histograms of $\Psi_{pp}^{\rm eff}$ and $\Delta_{pp}^{\rm eff}$ shown as bar charts. (a) The standard deviation of $\Psi_{pp}^{\rm eff}$ is 0.04° at average of 3.05°. (b) The standard deviation of $\Delta_{pp}^{\rm eff}$ is 0.3° at average of 100.2°.

B. Results

To test the performance of the system, we took data for more than 200 periods of rotations of the analyzer. The resulted standard deviations (shown in Fig. 4) of $\Psi_{pp}^{\rm eff}$ and $\Delta_{pp}^{\rm eff}$ are 0.04° and 0.3°(while Ψ_{pp}^{σ} and Δ_{pp}^{σ} are ~0.25° and 0.3°) for $\Psi_{pp}^{\rm eff} = 3.05°$, $\Delta_{pp}^{\rm eff} = 100.2°$, and $P = 4°$. We can then use the standard deviations ($d\Psi_{pp}^{\rm eff}$ and $d\Delta_{pp}^{\rm eff}$) and the known parameters (α, β, and dA) to obtain the intensity fluctuation δ, defined as dI/I_D in Appendix A, using the coupled equations (A3a) and (A3b). We found that the contribution of δ is larger than that of the error of the analyzer angle dA and the residue from the asymmetry of A_i in real measurements. It can be attributed to the mechanical vibration through such a long framework of the insert. Although the random errors are not as small as that of conventional ellipsometers, the precision of this system is good enough for many of the proposed studies,[4–8] and more importantly, it can be operated at much higher magnetic fields than the ones reported previously.

The Ψ_{pp}^{σ} and Δ_{pp}^{σ} spectra of GaAs substrate from 1.514 to 1.532 eV at 4.2 K are shown in Figs. 5(a) and 5(b), respectively for different magnetic fields up to 14 T. In Fig. 5(b), the asymmetric curves in Δ_{pp}^{σ} spectra across the 180° line indicate that the phase differences change sign, from right-handed (negative helicity) to left-handed (positive helicity) polarizations,[22] near the transitions. The raw RAE data with

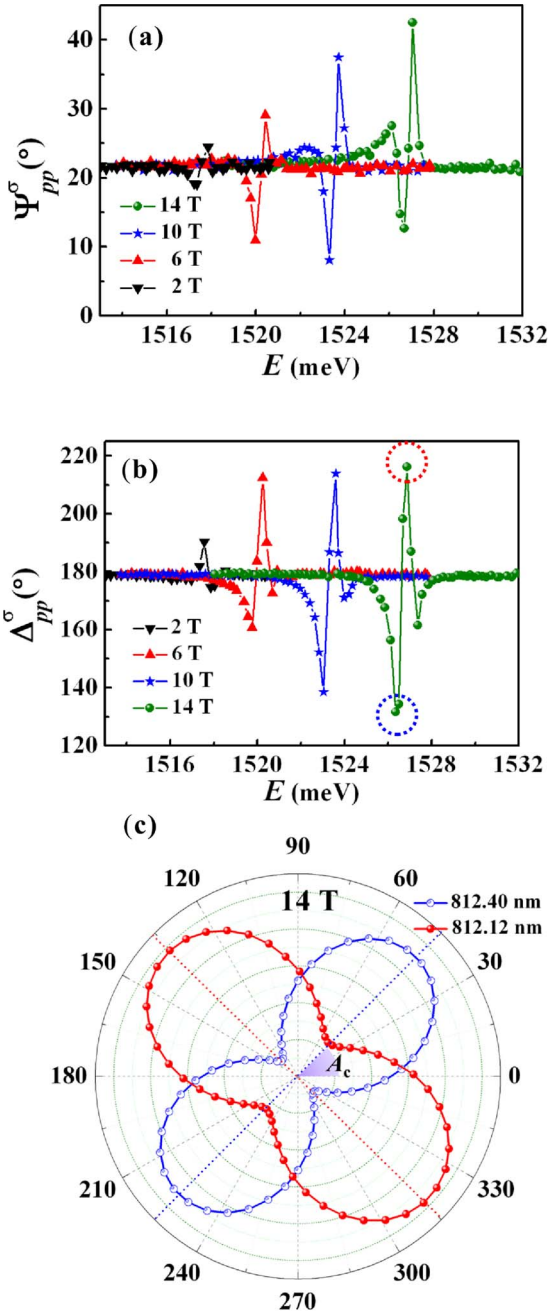

FIG. 5. Spectra of (a) Ψ_{pp}^{σ} and (b) Δ_{pp}^{σ} of intrinsic GaAs substrate for different magnetic fields at 4.2 K. (c) Intensity versus analyzer angle at 812.12 nm (solid points) and 812.40 nm (open circles) in polar coordinates at 14 T. The angle A_c is defined in Appendix C.

a quarter-wave plate in front of the rotating analyzer at wavelength 812.12 nm and 812.4 nm (marked by the dashed circles in Fig. 5(b)) are plotted in a polar coordinate in Fig. 5(c). The sign change of Δ_{pp}^{σ} can be determined from the orientations of the long-axes (the dashed-lines) of the polar curves located in different quadrants (see Appendix C).

C. Data analysis and discussion

To simulate the spectra of R_{pp}, we use the exciton-polariton model with spatial dispersion[23,24] to calculate the reflection coefficients of p- and s- polarization components,

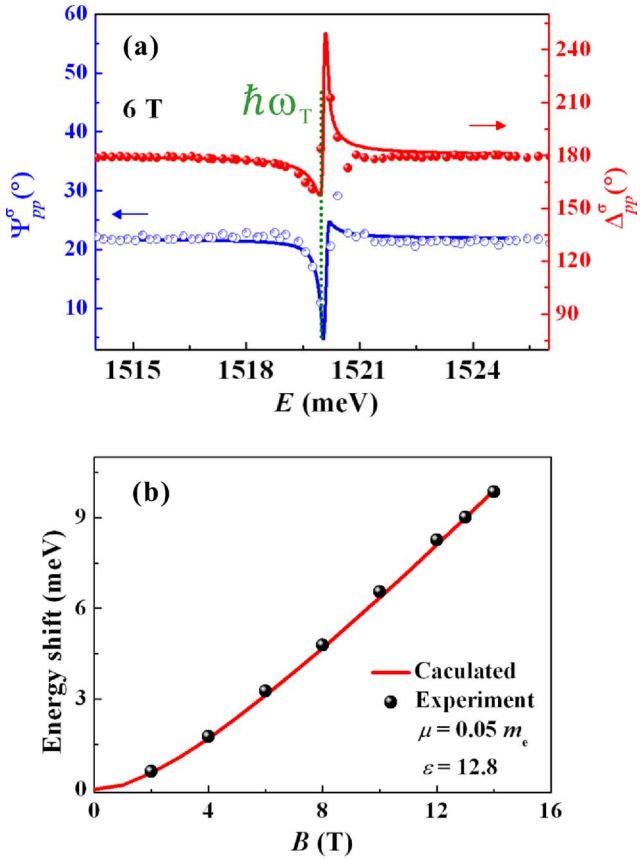

FIG. 6. (a) Measured (points) and calculated spectra (lines) of Ψ^{σ}_{pp} (left-axis) and Δ^{σ}_{pp} (right-axis) at 6 T. The parameters used are: $\hbar\omega_T = 1.52$ eV, $\hbar\nu = 0.1$ meV, $\hbar\omega_p = 0.07$ eV, $M = 0.298\ m_e$,[27] $d_I = 40$ nm, and Pekar's ABC.[25,28] (b) Energy shift versus magnetic field. The black points is obtained by the shape fitting ($\hbar\omega_T$), and the line is fitted by the result of the Schrödinger equation with a reduced effective mass $\mu = 0.05\ m_e$[31] and a dielectric constant $\epsilon = 12.8$.[32]

respectively. The dielectric function of spatial dispersive media can be expressed as[23,24]

$$\varepsilon(\mathbf{q},\omega) = \varepsilon_b + \frac{\omega_p^2}{\omega_T^2 + Dq^2 - \omega^2 - i\nu\omega}, \tag{12}$$

where ε_b is the background dielectric constant, ω_p^2 and ω_T stand for the transition strength and frequency, ν is the damping parameter, $D = \hbar\omega_T/M$ (M is the center-of-motion effective mass of the exciton) describes the spatial non-locality due to the exciton center-of-mass motion. Because of the spatial dispersion effect in Eq. (12), the quadratic of the wavevector q^2 for each frequency has two different solutions for the transverse mode and single solution for the longitudinal mode, respectively, as we solve Maxwell's equation

$$\mathbf{q}\times(\mathbf{q}\times\mathbf{E}) - \frac{\omega^2}{c^2}\varepsilon(\mathbf{q},\omega)\mathbf{E} = 0, \tag{13}$$

where $\mathbf{E}$ is the electric field in the medium, and c is the speed of light.[23,24] The multi-components (modes) of the electric field and the magnetic field are calculated in this spatial dispersive media and matched at the interfaces using the generalized additional boundary condition (ABC).[24,25] A exciton-free (dead) layer[24,26] with thickness d_I is introduced at the surface of the sample in our calculation. The result of the calculation at 6 T, as an example, is showed in Fig. 6(a).

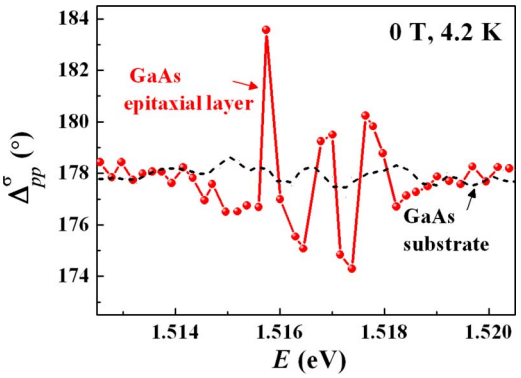

FIG. 7. Comparison of Δ^{σ}_{pp} spectra of GaAs substrate (dashed-line) and GaAs epitaxial layer (solid-line) grown by MBE at zero magnetic field.

The effects of external magnetic fields on the ellipsometry spectra were also investigated. The curves in Figs. 5(a) and 5(b) shift to higher energy and become stronger as magnetic fields increase. This can be explained by the diamagnetic effect of excitons and the increased oscillator strength due to the magnetic confinement.[29] The amount of diamagnetic shift depends on the radius of the magneto-excitons in the plane perpendicular to the magnetic field, and can be obtained by solving the Schrödinger equation under a magnetic field along the direction of the sample surface.[30] The calculated magnetic-field dependent ground state energy shift is shown in Fig. 6(b) and compared with the energy shift obtained by Ψ^{σ}_{pp} and Δ^{σ}_{pp} spectra fitting (Fig. 6(a)). The reduced effective mass μ and the dielectric constant ϵ used are $0.05\ m_e$[31] and 12.8,[32] respectively. However, we should mention that the calculation was only performed with the simple two-band hydrogen-like exciton in a magnetic field[30] and the Zeeman term, the motion of the exciton, and the electron-hole exchange interaction are neglected.

Semi-insulating GaAs substrates, because of the high defect density, usually have broadened spectra due to a large damping. Thus it is difficult to observe the fine structure of level splitting at high fields and even the signal from the zero-field exciton becomes very weak. In comparison, we show the ellipsometric measurement of a high-quality GaAs layer grown by molecular beam epitaxy (MBE). The layer, grown on a (100) semi-insulating GaAs substrate, was undoped and had a thickness of 1 μm. Unlike what was seen from the substrate alone, the result from the epilayer shows discernible features in the ellipsometry spectra even at zero magnetic field as shown in Fig. 7, and some of the features exhibit intriguing behaviors when high magnetic fields are applied. These features, which have not been reported before, can now be studied and observed using our ellipsometry system. The data and more detailed analysis will be reported in Ref. 33.

IV. CONCLUSION

In conclusion, we have demonstrated an ellipsometry system that can be fitted into a long-neck He-dewar with a high-field superconducting magnet. The functionality and the

precision of the system were systematically analyzed. Its random error was found to be dominated by the light intensity fluctuation. To demonstrate the system's capability, we have measured the ellipsometry spectra of GaAs samples with and without an epilayer near the band edge in magnetic fields up to 14 T. Fine structures from the high quality GaAs epilayer was observed for the first time. With its unique capability, this system will allow us to study the collective magneto-optical response of metamaterials consisting of semiconductor nano-objects and the behavior of exciton-polariton propagation under high magnetic fields at low temperatures.

ACKNOWLEDGMENTS

This work was supported by the National Science Council of the Republic of China under Contract No. NSC 102-2221-E-009-132-, Center for Nano Science and Technology of National Chiao Tung University, and National Nano Device Laboratories. We also thank Professor Y. F. Chao in Department of Photonics, National Chiao Tung University for numerous educational discussions.

APPENDIX A: ERROR ANALYSIS OF ELLIPSOMETRY PARAMETERS

The small fluctuations $d\Psi_{pp}^{\text{eff}}$ and $d\Delta_{pp}^{\text{eff}}$ can be obtained from the derivative of Eqs. (11a) and (11b).

$$d\Psi_{pp}^{\text{eff}} = \left[\frac{\cos^2\Psi_{pp}^{\text{eff}}\left(\tan^2 P + \tan^2\Psi_{pp}^{\text{eff}}\right)^2}{4\tan\Psi_{pp}^{\text{eff}}\tan^2 P}\right] d\alpha, \tag{A1a}$$

and

$$d\Delta_{pp}^{\text{eff}} = \frac{1}{\sin\Delta_{pp}^{\text{eff}}(1-\alpha^2)^{3/2}}[(\alpha^2-1)d\beta - (\alpha\beta)d\alpha]. \tag{A1b}$$

As $P \sim \Psi_{pp}^{\text{eff}}$ and $\Delta_{pp}^{\text{eff}} \sim 90°$($\alpha$ and $\beta \sim 0$ from Eqs. (11a) and (11b)), both $d\Psi_{pp}^{\text{eff}}$ and $d\Delta_{pp}^{\text{eff}}$ are minimized. That is, for a rotating-analyzer ellipsometer, a better precision can be achieved if the light before the rotating analyzer is nearly circular polarized, i.e., $P \sim \Psi_{pp}^{\text{eff}}$ and $\Delta_{pp}^{\text{eff}} \sim 90°$.

The small fluctuations of the Fourier coefficients $d\alpha$ and $d\beta$ can be derived from Eq. (10). The Fourier coefficients α', β' and the average intensity I_D' with small fluctuations of the intensities dI_i and the analyzer angles dA_i ($i = 1, 2, 3, \ldots N$) can be written as

$$\alpha' = \frac{2}{I_D' N}\sum_{i=1}^{N}(I_i + dI_i)\cos[2(A_i + dA_i)], \tag{A2a}$$

and

$$\beta' = \frac{2}{I_D' N}\sum_{i=1}^{N}(I_i + dI_i)\sin[2(A_i + dA_i)]. \tag{A2b}$$

We assume that the fluctuations of intensities and analyzer angles are both constants, i.e., $dI_i = dI_D = dI$ and $dA_i = dA$, for each analyzer angle A_i when α, β are small ($I_i \sim I_D$). By expanding the equations above and dropping the smallest terms, we can obtain

$$d\alpha = \frac{-\delta}{1+\delta}\alpha + \frac{-\sin 2dA}{1+\delta}\beta + \frac{\delta}{1+\delta}\frac{2}{N}\sum_{i=1}^{N}\cos 2A_i, \tag{A3a}$$

and

$$d\beta = \frac{-\delta}{1+\delta}\beta + \frac{-\sin 2dA}{1+\delta}\alpha + \frac{\delta}{1+\delta}\frac{2}{N}\sum_{i=1}^{N}\sin 2A_i, \tag{A3b}$$

where δ is defined as dI/I_D. If A_i are chosen symmetrically (i.e., A_i and A_i +180° for $A_i < 90°$), the last term in both Eqs. (A3a) and (A3b) becomes zero. The related parameters causing the error of the Fourier coefficients are the intensity fluctuation δ, the random error of the analyzer angle dA, the random choice of the analyzer angles (the last summation terms of Eqs. (A3a) and (A3b)) and the choice of the polarizer angle P.

APPENDIX B: PRECISION OF THE MULTI-REFLECTION RAE

For precise detection of the changes of R_{pp}^{σ} of the measured spectra under various external magnetic fields, to minimize the random error of the RAE technique with a

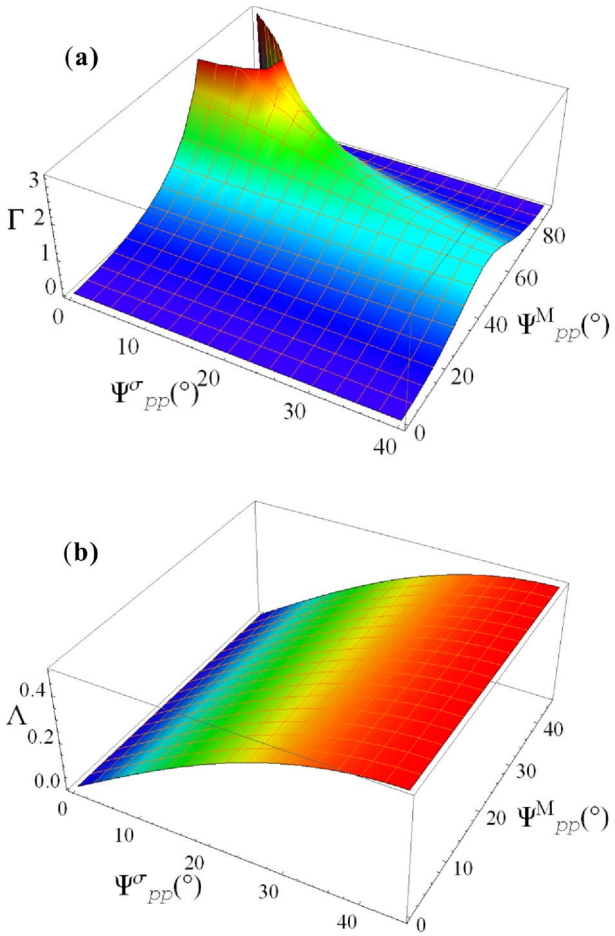

FIG. 8. Γ (a) and Λ (b) (in Eqs. (B1) and (B3)) as a function of Ψ_{pp}^{σ} and Ψ_{pp}^{M}.

TABLE I. Maximum and minimum values of the elliptical intensity distribution (Eq. (9a)) for A_c in different domains.

Domain	β/α	Maximum ($\beta \geq 0$)	Minimum ($\beta \leq 0$)
$0^\circ \leq 2A_c < 90^\circ$	≥ 0	$1 + \alpha\cos 2A_c + \beta\sin 2A_c$	$1 - \lvert\alpha\rvert\cos 2A_c - \lvert\beta\rvert\sin 2A_c$
$90^\circ \leq 2A_c \leq 180^\circ$	≤ 0	$1 + \lvert\alpha\rvert\lvert\cos 2A_c\rvert + \beta\sin 2A_c$	$1 - \alpha\lvert\cos 2A_c\rvert - \lvert\beta\rvert\sin 2A_c$

multi-reflection configuration is important. It can be shown that making the light before the rotating analyzer circularly polarized gives better precision for RAE[21] (see Appendix A). Therefore, we choose a polarizer angle P close to the measured ellipsometry angle Ψ_{pp}^{eff} to balance the intensities of p- and s-polarized components after three times of reflection.

To analyze the precision of the measured result, we first find the relationship between the error of Ψ_{pp}^{eff} and the error of Ψ_{pp}^{σ} by taking the derivative of the real part of Eq. (7a).

$$d\Psi_{pp}^{\text{eff}} = \frac{\sec^2 \Psi_{pp}^{\sigma} \tan^2 \Psi_{pp}^{\text{M}}}{1 + \tan^2 \Psi_{pp}^{\sigma} \tan^2 \Psi_{pp}^{\text{M}}} d\Psi_{pp}^{\sigma} \equiv \Gamma d\Psi_{pp}^{\sigma}, \tag{B1}$$

where Γ represents the coefficient that relates the two error quantities. Figure 8(a) shows Γ as a function of Ψ_{pp}^{σ} and Ψ_{pp}^{M}. For a given error in the triple reflection measurement, the error in the sample's parameter can be minimized by choosing proper Ψ_{pp}^{σ} and Ψ_{pp}^{M} to maximize Γ. Thus, we can choose the mirrors once we know the dielectric constant of the sample. For example, if Ψ_{pp}^{σ} equals 22° (for GaAs at a wavelength near 800 nm and a 60° incident angle), we can choose Ψ_{pp}^{M} close to 45° (see Fig. 8(a)) to minimize the error ($d\Psi_{pp}^{\sigma}$) of the deduced sample parameter.

However, the error in the triple reflection measurement, $d\Psi_{pp}^{\text{eff}}$, depends on the polarizer angle P and is related to the error in the Fourier component α by (see Appendix A)

$$d\Psi_{pp}^{\text{eff}} = \left[\frac{\cos^2 \Psi_{pp}^{\text{eff}} \left(\tan^2 P + \tan^2 \Psi_{pp}^{\text{eff}}\right)^2}{4 \tan \Psi_{pp}^{\text{eff}} \tan^2 P}\right] d\alpha. \tag{B2}$$

By using this relationship and choosing $P = \Psi_{pp}^{\text{eff}}$ for best precision, Eq. (B1) can be rewritten as

$$d\Psi_{pp}^{\sigma} = \frac{\tan^2 \Psi_{pp}^{\text{M}} \tan \Psi_{pp}^{\sigma}}{\Gamma\left[1 + \left(\tan^2 \Psi_{pp}^{\text{M}} \tan \Psi_{pp}^{\sigma}\right)^2\right]} d\alpha \equiv \Lambda d\alpha. \tag{B3}$$

The error $d\Psi_{pp}^{\sigma}$ is now related to the error in the Fourier coefficient $d\alpha$ (see Appendix A) by a factor Λ, which depends on the parameter Γ and the Ψ_{pp} values of the mirrors and the sample. Figure 8(b) shows the factor Λ as a function of Ψ_{pp}^{σ} and Ψ_{pp}^{M}. For a typical sample (i.e., $\Psi_{pp}^{\text{GaAs}} \sim 22^\circ$), Λ is a slowly varying function of Ψ_{pp}^{M}. The precision is not sensitive to the choice of a mirror when the polarizer angle P is chosen close to Ψ_{pp}^{eff}.

The precision of the phase difference Δ_{pp} can be shown as (see Eq. (A1b) in Appendix A)

$$d\Delta_{pp}^{\text{eff}} = \frac{1}{\sin \Delta_{pp}^{\text{eff}} (1 - \alpha^2)^{3/2}} [(\alpha^2 - 1)d\beta - (\alpha\beta)d\alpha]. \tag{B4}$$

It can be improved by adding a quarter-wave plate in front of the analyzer especially for measuring dielectric samples whose Δ_{pp} is close to 0° or 180°. Then, Eq. (11b) becomes

$$\sin \Delta_{pp}^{\text{eff}} = -\text{sgn}(P) \frac{\beta}{\sqrt{1 - \alpha^2}} \tag{B5}$$

for the fast axis of a quarter-wave plate parallel to the incident plane. From Eq. (B5), the sign of Δ_{pp} can be distinguished by adding a quarter-wave plate in front of a rotating analyzer. This is important especially for the measurements with photon energy close to the exciton or polariton states (see Sec. III).

APPENDIX C: EXTREME VALUE AND ITS CORRESPONDING ANALYZER ANGLE OF A RAE INTENSITY DISTRIBUTION

To find out the maximum/minimum intensity of an ellipse and the corresponding analyzer angle A_c, we differentiate Eq. (9a) with respect to A. The angle A_c satisfies the relation

$$\tan(2A_c) = \frac{\beta}{\alpha}. \tag{C1}$$

Substituting Eqs. (C1), (11a), and (11b) into Eq. (9a) and analyzing the sign of Eq. (9a) (see Table I), we can find that the maximum intensity will be in the first and the third quadrants if $0^\circ \leq \Delta_{pp} < 90^\circ (\beta \geq 0)$, and in the second and the fourth quadrants if $90^\circ \leq \Delta_{pp} \leq 180^\circ (\beta \leq 0)$.

Because the domain of Δ_{pp} is in the range of 0° to 180° for $\cos \Delta_{pp}$ in Eq. (11b), we cannot distinguish whether Δ_{pp} is larger than 180° or not. For example, $\Delta_{pp} = 150^\circ$ and $\Delta_{pp} = 210^\circ (-150^\circ)$ show exactly the same elliptical intensity distribution for an identical Ψ_{pp}. However, if a quarter-wave plate is added in front of a rotating analyzer, the maximum intensities will be in different quadrants, and thus the Δ_{pp} values can be identified.

[1] R. Azzam and N. Bashara, *Ellipsometry and Polarized light* (North-Holland, Amsterdam, 1989).
[2] D. Goldstein, *Polarized Light*, 2nd ed. (Marcel Dekker, Inc., New York, 2003).
[3] H. Tompkins and E. A. Irene, *Handbook of Ellipsometry* (Elsevier, 2005).
[4] O. Voskoboynikov, C. M. J. Wijers, J. L. Liu, and C. P. Lee, Phys. Rev. B **71**, 245332 (2005).
[5] C. M. J. Wijers, J. H. Chu, J. L. Liu, and O. Voskoboynikov, Phys. Rev. B **74**, 035323 (2006).
[6] C. M. J. Wijers, O. Voskoboynikov, and J. L. Liu, Phys. Status Solidi C **3**, 3782 (2006).
[7] L. M. Thu and O. Voskoboynikov, Phys. Rev. B **80**, 155442 (2009).
[8] O. Voskoboynikov, Int. J. Multiscale Comput. Eng. **8**, 195 (2010).
[9] J. Tignon, T. Hasche, D. S. Chemla, H. C. Schneider, F. Jahnke, and S. W. Koch, Phys. Rev. Lett. **84**, 3382 (2000).
[10] H. C. Schneider, F. Jahnke, S. W. Koch, J. Tignon, T. Hasche, and D. S. Chemla, Phys. Rev. B **63**, 045202 (2001).

[11]S. Schumacher, G. Czycholl, and F. Jahnke, Phys. Status Solidi B **234**, 172 (2002).
[12]S. Schumacher, G. Czycholl, F. Jahnke, I. Kudyk, H. Rückmann, J. Gutowski, A. Gust, G. Alexe, and D. Hommel, Phys. Rev. B **70**, 235340 (2004).
[13]D. Schiumarini, N. Tomassini, L. Pilozzi, and A. D'Andrea, Phys. Rev. B **82**, 075303 (2010).
[14]A. Berger and M. Pufall, Appl. Phys. Lett. **71**, 965 (1997).
[15]G. Neuber, R. Rauer, J. Kunze, T. Korn, C. Pels, G. Meier, U. Merkt, J. Backstrom, and M. Rubhausen, Appl. Phys. Lett. **83**, 4509 (2003).
[16]M. Schubert, T. Hofmann, and C. M. Herzinger, J. Opt. Soc. Am. A **20**, 347 (2003).
[17]T. Hofmann, U. Schade, C. M. Herzinger, P. Esquinazi, and M. Schubert, Rev. Sci. Instrum. **77**, 063902 (2006).
[18]K. Mok, N. Du, and H. Schmidt, Rev. Sci. Instrum. **82**, 033112 (2011).
[19]M. Schubert, B. Rheinlnder, J. A. Woollam, B. Johs, and C. M. Herzinger, J. Opt. Soc. Am. A **13**, 875 (1996).
[20]W. Budde, Appl. Opt. **1**, 201 (1962).
[21]D. E. Aspnes, J. Opt. Soc. Am. A **21**, 403 (2004).
[22]J. D. Jackson, *Classical Electrodynamics*, 3rd ed. (John Wiley & Sons, New Jersey, 1998), p. 300.
[23]J. J. Hopfield and D. G. Thomas, Phys. Rev. **132**, 563 (1963).
[24]G. H. Cocoletzi and W. L. Mochán, Surf. Sci. Rep. **57**, 1 (2005).
[25]P. Halevi and R. Fuchs, J. Phys. C **17**, 3869 (1984).
[26]D. D. Sell, S. E. Stokowski, R. Dingle, and J. V. DiLorenzo, Phys. Rev. B **7**, 4568 (1973).
[27]B. Flores-Desirena, F. Pérez-Rodriguez, and P. Halevi, Phys. Rev. B **50**, 5404 (1994).
[28]S. Pekar, Sov. J. Exp. Theor. Phys. **6**, 785 (1958).
[29]T. Tanaka, Z. Zhang, M. Nishioka, and Y. Arakawa, Appl. Phys. Lett. **69**, 887 (1996).
[30]J. Singh, *Physics of Semiconductors and Their Heterostructures* (McGraw-Hill, New York, 1993), pp. 703–707.
[31]S. B. Nam, D. C. Reynolds, C. W. Litton, R. J. Almassy, and T. C. Collins, Phys. Rev. B **13**, 761 (1976).
[32]J. S. Blakemore, J. Appl. Phys. **53**, R123 (1982).
[33]S. K. Su, O. Voskoboynikov, L. C. Li, Y. W. Suen, and C. P. Lee, "GaAs polariton propagation in magnetic field: Oblique incident ellipsometry measurement" (unpublished).